State of stress in the Permian Basin, Texas and New Mexico: Implications for induced seismicity

Jens-Erik Lund Snee[1] and Mark D. Zoback[1]

Abstract

Since the 1960s, the Permian Basin of west Texas and southeast New Mexico has experienced earthquakes that were possibly triggered by oil and gas activities. In recent years, seismicity has been concentrated near Pecos, Texas; around the Dagger Draw Field, New Mexico; and near the Cogdell Field, Snyder, Texas. We have collected hundreds of measurements of stress orientation and relative magnitude to identify potentially active normal, normal/strike-slip, or strike-slip faults that might be susceptible to earthquake triggering in this region. In the Midland Basin and Central Basin Platform, the faulting regime is consistently normal/strike slip, and the direction of the maximum horizontal compressive stress (S_{Hmax}) is approximately east–west, although modest rotations of the S_{Hmax} direction are seen in some areas. Within the Delaware Basin, however, a large-magnitude clockwise rotation (~150°) of S_{Hmax} occurs progressively from being nearly north–south in the north to east-southeast–west-northwest in the south, including the western Val Verde Basin. A normal faulting stress field is observed throughout the Delaware Basin. We use these stress data to estimate the potential for slip on mapped faults across the Permian Basin in response to injection-related pressure changes at depth that might be associated with future oil and gas development activities in the region.

Introduction

The Permian Basin of west Texas and southeast New Mexico is one of the most important petroleum-producing regions in the United States, containing numerous vertically stacked producing intervals (Dutton et al., 2005). The basin is subdivided into several structural regions (Figure 1), including the prolific Midland and Delaware basins, which are separated by the Central Basin Platform, a crystalline-basement-involved structural high overlain by carbonate reef deposits and clastic rocks (Cartwright, 1930; Galley, 1958; Matchus and Jones, 1984).

Fluid injection and hydrocarbon production have been suspected as the triggering mechanisms for numerous earthquakes that have occurred in the Permian Basin since the 1960s (Rogers and Malkiel, 1979; Keller et al., 1981; Orr, 1984; Keller et al., 1987). The area is also naturally seismically active (Doser et al., 1991, 1992). Seismicity in the Permian Basin has historically occurred in several localized areas (Figure 1), including parts of the Central Basin Platform and around the Dagger Draw and Cogdell fields (Sanford et al., 2006; Gan and Frohlich, 2013; Pursley et al., 2013; Herzog, 2014; Frohlich et al., 2016). Since about 2009, seismicity has occurred in the southern Delaware Basin (Jing et al., 2017), an area where the USGS National Earthquake Information Center and Keller et al. (1987) report very little previous seismicity. Since the TexNet Seismological Network (Savvaidis et al., 2017) began recording earthquakes across Texas in January 2017, at least three groups of earthquakes, surrounded by more diffusely located events, have occurred in the southern Delaware Basin, near Pecos, Texas. A fourth group of events occurred mostly in mid-November 2017 farther to the west in northeastern Jeff Davis County. In addition, a group of mostly small ($M_L < 2$) earthquakes occurred between Midland and Odessa, in the Midland Basin.

As illustrated through recent studies of induced seismicity in Oklahoma (Walsh and Zoback, 2016), knowledge of the current state of stress is an essential component in estimating the pore-pressure perturbation needed to trigger an earthquake on a given fault. Such analyses enable both retrospective analyses of potential triggering conditions of past earthquakes as well as estimates of the likelihood of future slip on mapped faults due to fluid injection or extraction. As part of our work to map the state of stress in Texas, we (Lund Snee and Zoback, 2016) recently contributed more than 100 new, reliable (A–C-quality) maximum horizontal compressive stress (S_{Hmax}) orientations specifically within the Permian Basin, together with an interpolated map of the relative principal stresses expressed using the A_ϕ parameter (Simpson, 1997). In anticipation of fluid-injection activities associated with the thousands of wells to be drilled in the Permian Basin in the next few years, we report more than 100 additional S_{Hmax} orientations and a refined map of the relative stress magnitudes (Figure 1) to provide a comprehensive view of the state of stress in the Permian Basin and its relation to potential earthquake triggering on faults in the region.

In this paper, we first summarize the compilation of new stress measurements and provide an overview of relative stress magnitudes. We then discuss the stress field (especially in areas where it varies considerably, such as the Delaware Basin) and apply the new stress data to estimate the fault slip potential that would be expected due to fluid-pressure increases that might be associated with fluid injection at depth. This analysis will utilize FSP v.1.07, a freely available software tool developed by the Stanford Center for Induced and Triggered Seismicity in collaboration with ExxonMobil (Walsh et al., 2017). We use only publicly available information about faults in the region.

Methods

In the earth, a combination of tectonic driving forces and local factors such as density heterogeneities give rise to anisotropic principal stresses with consistent orientations and relative magnitudes throughout the brittle upper crust (Zoback and Zoback, 1980; Zoback, 1992). These principal stresses, which are continually replenished by tectonic activity, are modulated by the finite strength of the crust, which dissipates accumulated stresses through seismic and aseismic slip on faults. Consequently, most of the brittle crust is thought to be critically stressed, meaning

[1]Stanford University, Department of Geophysics.

https://doi.org/10.1190/tle37020127.1.

that it is in a state of frictional equilibrium in which the faults best oriented for slip with respect to the principal stress directions are usually within one earthquake cycle of failure (Zoback et al., 2002). Thus, knowing the orientations of the principal stresses reveals the faults that are most likely to slip. Conveniently, one principal stress is usually vertical and the other two horizontal (Zoback and Zoback, 1980) because the earth's surface is an interface between a fluid (air or water) and rock, across which no shear tractions are transmitted. Knowing both the orientation of S_{Hmax} and the relative magnitudes of the principal stresses is therefore sufficient to predict the orientations (strike and dip) and type (normal, strike slip, and/or reverse) of faults most likely to slip.

Measuring the orientation and relative magnitudes of the principal stresses. (*Editor's note: Figures A1 and A2 and Tables A1–A5 are included as supplemental material to this paper in SEG's Digital Library at https://library.seg.org/doi/suppl/10.1190/tle37020127.1.*) The S_{Hmax} orientations shown in Figure 1 and reported in supplemental Tables A1 and A2 were mostly measured using well-established techniques. The vast majority of these orientations represent means of the azimuths of drilling-induced tensile fractures (DITF) or wellbore breakouts observed using image logs such as the fullbore formation microimager (FMI) and ultrasonic borehole imager. As reported in the supplemental material that accompanies this article, the quality of each measurement was assessed using Fisher et al. (1987) statistics where possible. Quality ratings were assigned to each measurement using criteria provided in Table A3, which now include criteria for aligned microseismic events that define the orientations of hydraulic fractures. Our criteria are based on those presented by Zoback and Zoback (1989), Zoback (2010), and Alt and Zoback (2017), who specify that only A–C-quality data are sufficiently robust to justify plotting on a map (D-quality measurements are reported in Tables A1 and A2 but are not mapped). These quality criteria were developed to ensure that each mapped S_{Hmax} orientation is well constrained and is based on a sufficient number and depth range of measured stress indicators.

Six orientations, previously reported by Lund Snee and Zoback (2016) and included in Figure 1, were measured by averaging the

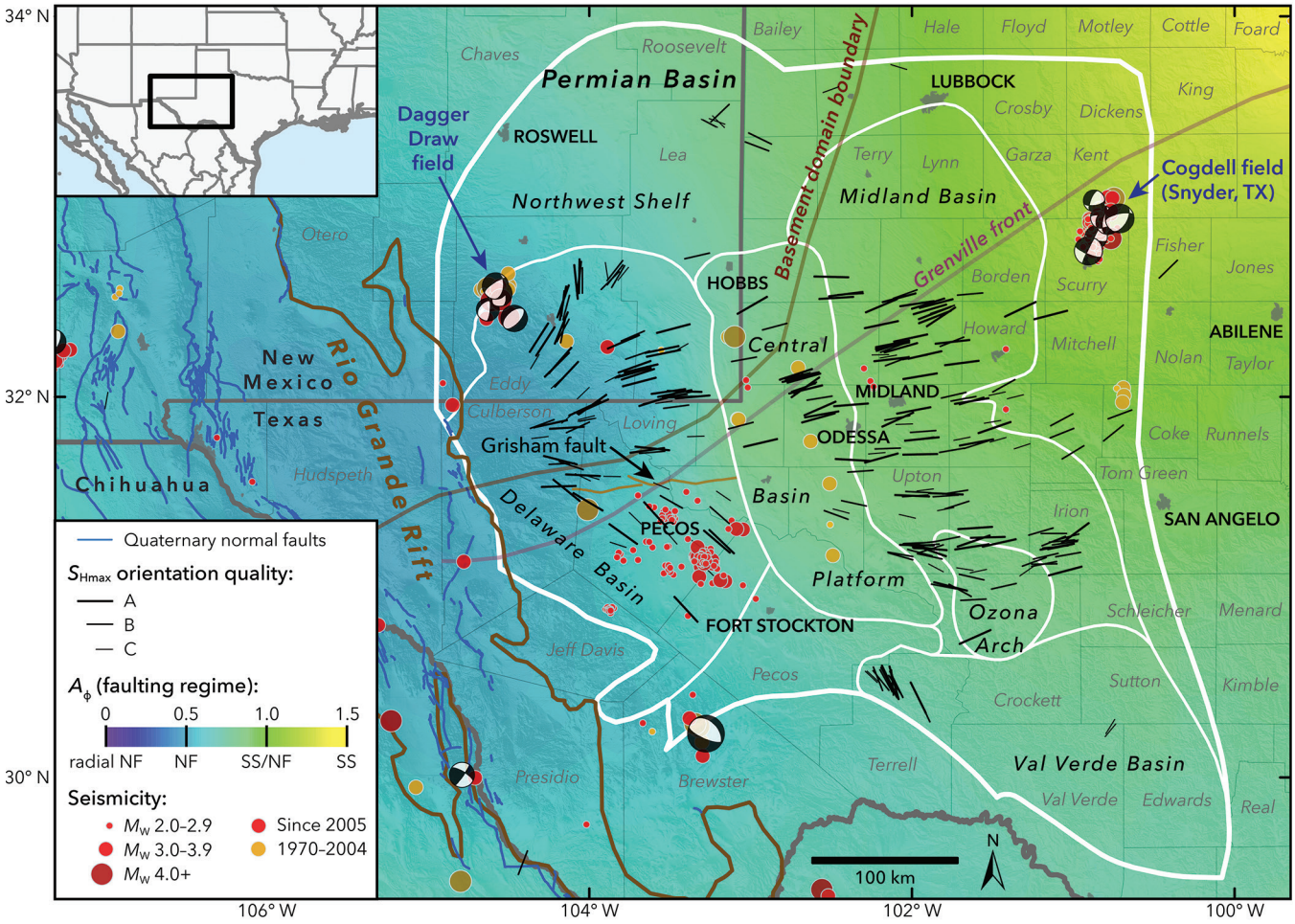

Figure 1. State of stress in the Permian Basin, Texas and New Mexico. Black lines are the measured orientations of S_{Hmax}, with line length scaled by data quality. The colored background is an interpolation of measured relative principal stress magnitudes (faulting regime) expressed using the A_ϕ parameter (see text for details) of Simpson (1997). Blue lines are fault traces known to have experienced normal-sense offset within the past 1.6 Ma, from the USGS Quaternary Faults and Folds Database (Crone and Wheeler, 2000). The boundary between the Shawnee and Mazatzal basement domains is from Lund et al. (2015), and the Precambrian Grenville Front is from Thomas (2006). The Permian Basin boundary is from the U.S. Energy Information Administration, and the subbasin boundaries are from the Texas Bureau of Economic Geology Permian Basin Geological Synthesis Project. Earthquakes are from the USGS National Earthquake Information Center, the TexNet Seismic Monitoring Program, and Gan and Frohlich (2013). Focal mechanisms are from Saint Louis University (Herrmann et al., 2011).

horizontal azimuth of the fastest shear-wave propagation in subvertical wells using measurements from crossed-dipole sonic logs. We also include several new S_{Hmax} orientations that were obtained from formal inversions of focal mechanisms from microseismic events detected during hydraulic fracturing operations. Several other S_{Hmax} orientations were obtained by measuring the orientations of aligned microseismic events thought to represent propagating hydraulic fractures. When collecting stress measurements from microseismic data, we do not account for the possibility of localized changes of stress orientations that might develop as a result of fracturing and proppant emplacement. It is unlikely that stimulation-induced changes in stress orientation would occur except in areas of very low stress anisotropy (which we demonstrate are rare). In such areas, there would not be consistent microseismic alignments orthogonal to the least principal stress that would satisfy the quality-control criterion for reliable stress orientations that we have developed (Table A3).

In addition to our new data, Figure 1 also includes previously published S_{Hmax} orientations from the Permian Basin area that we consider reliable. The 2016 release of the World Stress Map (Heidbach et al., 2016) included only a handful of S_{Hmax} orientations in the Permian Basin. We have downgraded the quality ratings for two older measurements that we suspect were made on the basis of mistaken interpretations. A large collection of S_{Hmax} orientations published by Tingay et al. (2006) and included in the World Stress Map Database were given D-quality ratings due to the lack of sufficient quality information (e.g., depth ranges, number of fractures, or standard deviations of fracture orientations), although many are in agreement with high-quality nearby measurements we utilize. Previously unpublished information contributed by R. Cornell (personal communication) is reported in Table A1, but there is not sufficient quality information to upgrade any of his measurements to C quality and be included in Figure 1. We also include S_{Hmax} orientations recently published by Forand et al. (2017), who report S_{Hmax} patterns consistent with the variations shown by Lund Snee and Zoback (2016). Although Forand et al. (2017) do not list the number and depth intervals for the stress indicators that they present, this information is included in their map because the distributions of fracture orientations shown in their rose diagrams allow us to interpret means, standard deviations, and the minimum number of fractures.

We interpolate the relative principal stress magnitudes across this area (colored background in Figure 1) using measurements reported in Table A4. We choose to represent the relative magnitudes of the three principal stresses (S_V, S_{Hmax}, and S_{hmin}) using the A_ϕ parameter (Simpson, 1997). The A_ϕ parameter (explained graphically in Figure A1) conveniently describes the ratio between the principal stress magnitudes using a single, readily interpolated value that ranges smoothly from 0 (the most extensional possible condition of radial normal faulting) to 3 (the most compressive possible condition of radial reverse faulting). The parameter is defined mathematically by

$$A_\phi = (n + 0.5) + (-1)^n (\phi - 0.5), \quad (1)$$

where

$$\phi = \frac{S_2 - S_3}{S_1 - S_3}. \quad (2)$$

S_1, S_2, and S_3 are the magnitudes of the maximum, intermediate, and minimum principal stresses, respectively, and n is 0 for normal faulting, 1 for strike-slip faulting, and 2 for reverse faulting.

Probabilistic analysis of fault slip potential. As mentioned earlier, we utilize FSP v.1.07 (Walsh et al., 2017) to estimate the slip potential on faults throughout the Permian Basin. The FSP tool allows operators to estimate the potential that planar fault segments will be critically stressed within a local stress field. Critically stressed conditions occur when the ratio of resolved shear stress to normal stress reaches a failure criterion, in this case the linearized Mohr-Coulomb failure envelope. The FSP program allows for either deterministic or probabilistic geomechanical analysis of the fault slip potential, the former of which treats each input as a discrete value with no uncertainty range. The probabilistic geomechanics function estimates the FSP on each fault segment using Monte Carlo-type analysis to randomly sample specified, uniform uncertainty distributions for input parameters including the fault strike and dip, ambient stress field, rock properties, and initial fluid pressure.

We conducted our analysis on fault traces compiled from Ewing et al. (1990), Green and Jones (1997), Ruppel et al. (2005), and the USGS Quaternary Faults and Folds Database (Crone and Wheeler, 2000). Most of these databases do not specify fault dips, so we make the conservative assumption that, within the generally normal and normal/strike-slip faulting environment of the Permian Basin, all potentially active faults dip in the range of 50° to 90°. This assumption implies that all fault segments could be ideally oriented for slip in either normal or strike-slip faulting environments at reasonable coefficients of friction, depending on the alignment of their strike with respect to S_{Hmax} (Figure A1).

Here we apply the probabilistic geomechanics function of the FSP tool. We apply reasonable stress values and uncertainty ranges based on the variability of the stress field we observe within 16 study areas (listed in Table A5). The study areas were selected to represent fairly uniform A_ϕ values and S_{Hmax} orientations (Figure 2) to minimize spatial variations of stress field in any given study area. As an example, Figure A2 shows input parameter distributions sampled during FSP analysis for a random fault within Area 10.

For the purposes of this demonstration, we do not hydrologically model the pressure changes associated with any known injection scenario; we instead estimate the fault slip potential in response to an increase in the fluid-pressure gradient corresponding to a 4% increase relative to hydrostatic (0.4 MPa/km or 0.018 psi/ft) to evaluate the potential for relatively modest pressure changes in crystalline basement (2 MPa [300 psi] at 5 km [16,400 ft]) associated with produced water disposal. This is the same gradient of pore-pressure perturbation applied by Walsh and Zoback (2016) for FSP analysis in north-central Oklahoma. The eventual pore-pressure increase that will occur in the uppermost parts of the crystalline basement due to injection in this area is of course unknown, and it is important to note that *relative* differences in slip potential between differently oriented faults will remain the

same regardless of the magnitude of uniform pressure increase (although the absolute fault slip potential will vary). Operators interested in screening potential sites for wastewater injection wells, for example, might alternatively use the software to test specific scenarios of pore-pressure evolution with time due to injection from wells in a localized area. Although large portions of the Permian Basin are known to be overpressured and underpressured at certain stratigraphic intervals (e.g., Orr, 1984; Doser et al., 1992; Rittenhouse et al., 2016), for the sake of simplicity in this whole-basin demonstration, we initially assume hydrostatic conditions (P_p = 9.8 MPa/km ≈ 0.43 psi/ft). In general, hypocentral depths for potentially damaging injection-triggered earthquakes are within the upper crystalline basement (e.g., Zhang et al., 2013; Walsh and Zoback, 2015), for which little pore-pressure information is available but for which hydrostatic values are reasonable (Townend and Zoback, 2000).

State of stress in the Permian Basin

Figure 1 shows all reliable S_{Hmax} orientations and an interpolated view of the A_ϕ parameter across the Permian Basin. Throughout the Midland Basin, the eastern part of the Permian Basin, the stress field is remarkably consistent, with S_{Hmax} oriented ~east–west (with modest rotations of S_{Hmax} in some areas) and $A_\phi \approx 1.0$ (indicative of normal/strike-slip faulting). The stress field is more extensional in the Val Verde Basin to the south, with $A_\phi \approx 0.7$. Few S_{Hmax} orientations are presently available in that subbasin, but S_{Hmax} is northwest–southest in the western part of the basin and appears to be ~northeast–southwest in the central part of the basin. This is similar to the stress state seen farther to the southeast, where S_{Hmax} follows the trend of the growth faults that strike subparallel to the Gulf of Mexico coastline (Lund Snee and Zoback, 2016). Along the Central Basin Platform, S_{Hmax} is generally ~east–west but rotates slightly clockwise from east to west, with A_ϕ ~ 0.8–1.0. In the Delaware Basin, the stress field is locally coherent but rotates dramatically by ~150° clockwise from north to south across the basin. In the western part of Eddy County, New Mexico, S_{Hmax} is ~north–south (consistent with the state of stress in the Rio Grande Rift; Zoback and Zoback, 1980) but rotates to ~east-northeast–west-southwest in southern Lea County, New Mexico, and the northernmost parts of Culberson and Reeves counties, Texas. It should be noted that where rapid stress rotations are observed in the Delaware Basin are areas with low values of A_ϕ (indicative of relatively small differences between the horizontal stresses) and elevated pore pressure (Rittenhouse et al., 2016), making it possible for relatively minor stress perturbations to cause significant changes in stress orientation (e.g., Moos and Zoback, 1993).

S_{Hmax} continues to rotate clockwise southward in the Delaware Basin to become ~N155°E in western Pecos County, westernmost Val Verde Basin, and northern Mexico (Suter, 1991; Lund Snee and Zoback, 2016). On the Northwest Shelf, A_ϕ varies from ~0.5 (normal faulting) in north Eddy County to ~0.9 (normal and strike-slip faulting) further east. S_{Hmax} rotates significantly across the Northwest Shelf as well, from ~north–south in northwest Eddy County to ~east-southeast–west-northwest in northern Lea and Yoakum counties.

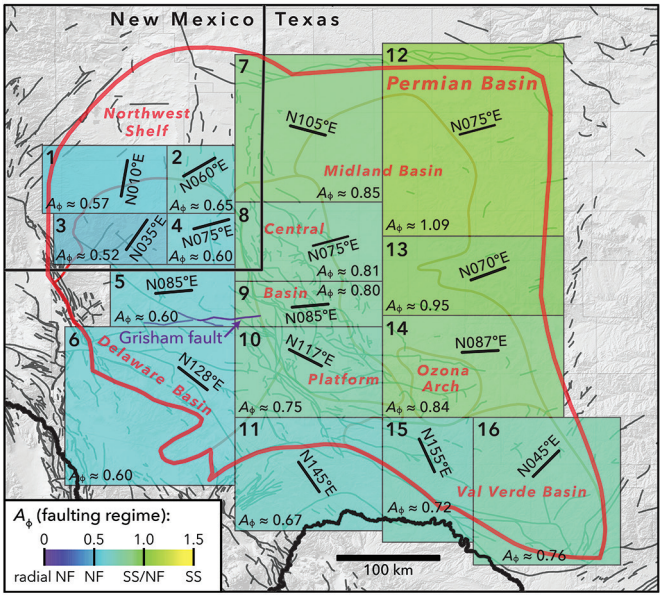

Figure 2. Map of study areas chosen for FSP analysis on the basis of broadly similar stress conditions. Text annotations indicate representative S_{Hmax} orientation and relative principal stress magnitudes (A_ϕ parameter) for each study area based on the data presented in Figure 1. Gray lines in the background indicate fault traces compiled from Ewing et al. (1990), Green and Jones (1997), Ruppel et al. (2005), and the USGS Quaternary Faults and Folds Database (Crone and Wheeler, 2000), to which we apply FSP analysis.

Slip potential on mapped faults

Figure 3 shows the results of our fault slip potential analysis for all study areas across the Permian Basin. We selected a color scale in which dark green lines represent faults with ≤5% probability of being critically stressed at the specified pore-pressure increase; dark red indicates faults with ≥45% fault slip potential; and yellow, orange, and light red represent intermediate values. The results shown in Figure 3 indicate that high fault slip potential is expected for dramatically different fault orientations across the basin, reflecting the varying stress field. In the northern Delaware Basin and much of the Central Basin Platform, for example, faults striking ~east–west are the most likely to slip in response to a fluid-pressure increase. However, farther south in the southern Delaware Basin, faults striking northwest–southeast are the most likely to slip, and ~east–west-striking faults have relatively low slip potential. Notably, we find high slip potential for large fault traces mapped across the southern Delaware Basin and Central Basin Platform, and along the Matador Arch. Figure 3 also indicates the faults that are *unlikely* to slip in response to a modest fluid-pressure increase. We find that large groups of mostly north–south-striking faults, predominantly located along the Central Basin Platform, the western Delaware Basin, and large parts of the Northwest Shelf have low fault slip potential at the modeled fluid-pressure perturbation. Knowing the orientations of faults that are unlikely to slip at a given fluid-pressure perturbation can be of great value because it provides operators with practical options for injection sites. Probabilistic geomechanical analysis of the type enabled by the FSP software is especially useful in areas with complex fault patterns. Figure 4 shows a larger-scale view of Area 10, an area of particularly dense faults. In Figure 4, it is clear that even

seemingly minor variations in fault strike can significantly change the fault slip potential.

Figures 3 and 4 illustrate the locations of earthquakes that have been recorded since 1970 in relation to the mapped faults. It is noteworthy that many earthquakes have occurred away from faults mapped at this regional scale, with the most obvious examples being groups of events described earlier, near the Dagger Draw Field (southeast New Mexico); the Cogdell Field (near Snyder, Texas); a group around the town of Pecos, Texas; and a recent group of mostly M < 2 events between the towns of Midland and Odessa, Texas. As the earthquakes undoubtedly occurred on faults, this observation underscores the necessity of developing improved subsurface fault maps, particularly for use in areas that might experience injection-related pore-pressure increases. Nevertheless, Figures 3 and 4 also show a number of earthquakes that may have occurred on mapped faults for which we estimate elevated fault slip potential. Of particular note are the recent (2009–2017) earthquakes in southeastern Reeves and northwestern Pecos counties, Texas, of which an appreciable number occurred on or near yellow or orange faults. Potentially active faults are identified near some towns in the Permian Basin, including Odessa (Figure 3) and Fort Stockton, Texas (Figure 4). In some areas, such as northern Brewster County, Texas, and parts of the northern Central Basin Platform, earthquakes occurred on or near orange or red faults that have relatively short along-strike lengths, making the faults appear fairly insignificant at this scale. In the area of active seismicity in Pecos and Reeves counties, we estimate relatively high slip potential for several significantly larger faults (>20 km along-strike length) on which few or no earthquakes have been recorded thus far (Figures 3 and 4). Larger faults are of particular concern for seismic hazard because they are more likely to extend into basement and, therefore, to potentially be associated with larger magnitude earthquakes.

As labeled in Figure 3, a number of regional-scale faults are known to exist in this area (Walper, 1977; Shumaker, 1992; Yang and Dorobek, 1995). The Permian Basin overlies a major boundary separating Precambrian-age lithospheric basement domains (Lund et al., 2015), and its crystalline "basement" hosts numerous major

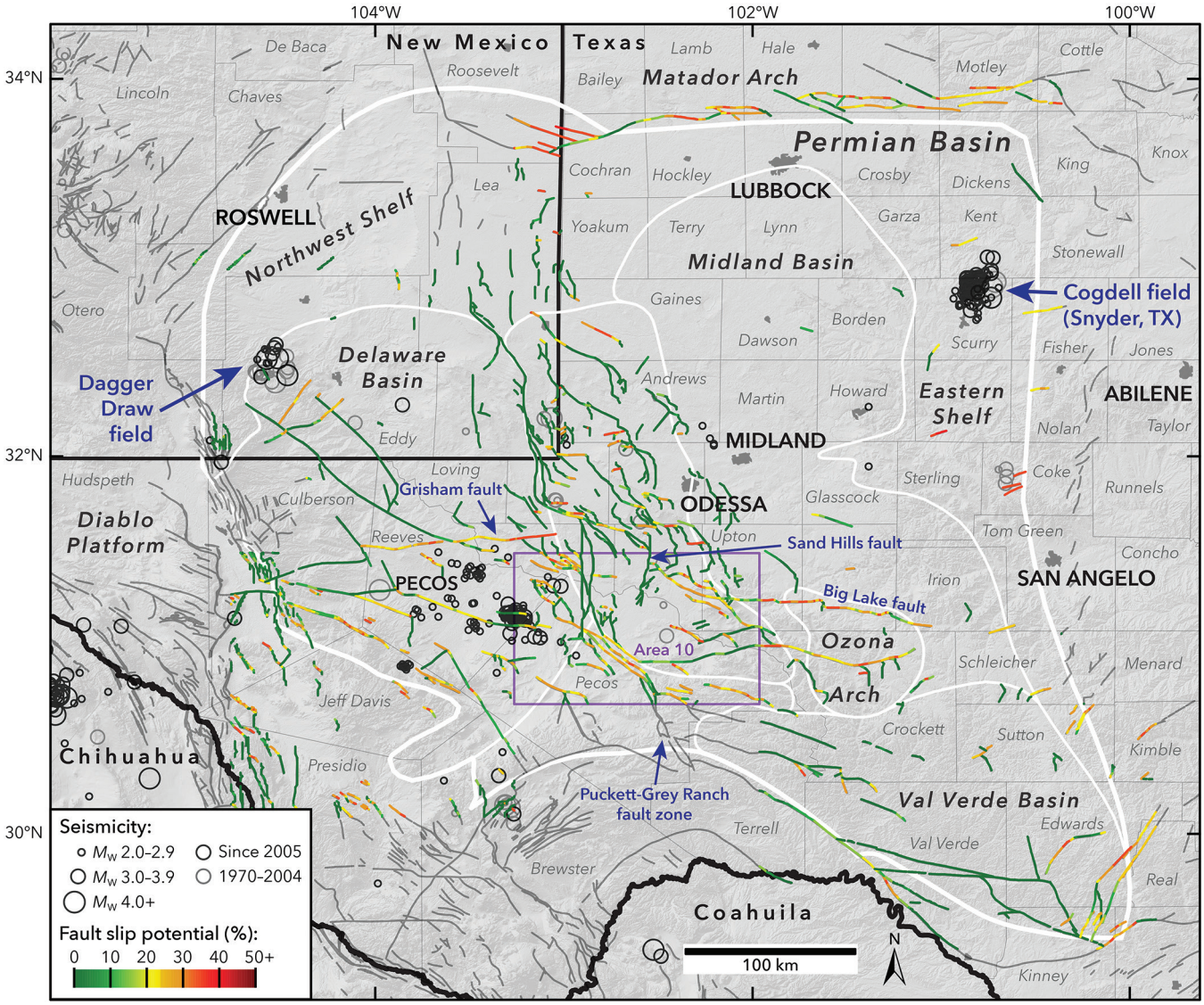

Figure 3. Results of our probabilistic FSP analysis across the Permian Basin. Data sources are as in Figures 1 and 2.

structures that have been repeatedly activated during subsequent plate collisions and rifting events (Kluth and Coney, 1981; Thomas, 2006). One notable example is the east–west-striking Grisham Fault (also referred to as the Mid-Basin Fault), which is between the rift margin of the Rodinia supercontinent and the boundary between the Shawnee and Mazatzal basement domains. The Grisham Fault is of particular importance for understanding the potential for induced seismicity in the Permian Basin because it is laterally extensive, offsets basement, and may have high slip potential. The upper part of Figure 5 (and Figure 3) shows a scenario in which the stresses resolved on the Grisham Fault are representative of Area 5, with S_{Hmax} oriented N085°E. However, the measured stress field changes dramatically from north to south across the Grisham Fault (Figures 1 and 2), presenting uncertainty about the stresses resolved upon the fault, reflected by its close proximity to Area 6, with a generalized S_{Hmax} orientation of N128°E. The lower part of Figure 5 shows the Grisham Fault in detail if the stress field shown in Area 6, just to the south, was appropriate. Needless to say, in the stress field represented by Area 5, fault segments oriented east–west are expected to have high probability of being critically stressed in response to a pore-pressure increase, but nearby west-northwest–east-southeast-striking faults have relatively low fault slip potential. In contrast, inclusion within the Area 6 stress field would result in low expected fault slip potential on the east–west segments but high values on the west-northwest–east-southeast-striking segments.

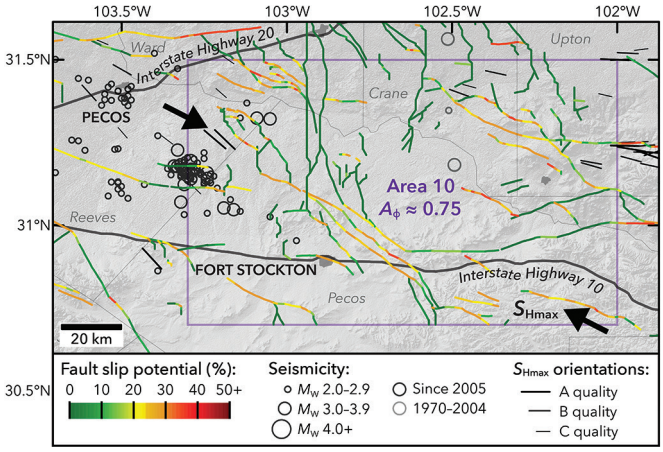

Figure 4. Large-scale view of the results of FSP analysis in Area 10 (location shown in Figures 2 and 3). Data sources are as in Figures 1 and 3.

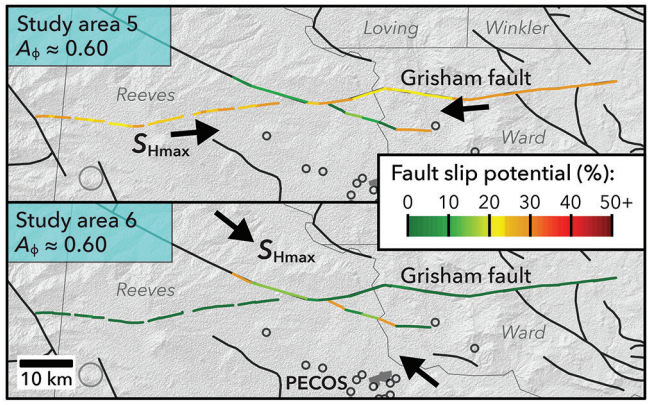

Figure 5. Map comparing the results of fault slip potential analysis on the Grisham (Mid-Basin) fault and selected nearby structures (locations shown in Figure 3) for stress conditions of Area 5 (S_{Hmax} N085°E ± 8°; top panel) and Area 6 (S_{Hmax} N128°E ± 15°; bottom panel). Symbols as in Figures 3 and 4.

The results shown in Figures 3–5 are not intended to provide a definitive view of the fault slip potential across this complex basin, nor do they constitute a seismic hazard map. While the stress field is complicated in this area, the changes in the stress field are coherent and mappable. We consider the greatest uncertainties in the map to be the lack of knowledge of subsurface faults and the magnitude and extent of potential pore-pressure changes in areas where increased wastewater injection may occur in the future, especially wastewater injection that might change pore pressure on basement faults. Operators wishing to use the FSP tool to screen sites for fluid injection should use detailed fault maps that are specific to the injection interval, the underlying basement, and any intervening units, which take into account geometric uncertainties.

Conclusions

As part of our stress mapping across the U.S. midcontinent, we have collected hundreds of S_{Hmax} orientations within the Permian Basin, and we also map the faulting regime across the region. Our new data reveal dramatic rotations of S_{Hmax} within the Delaware Basin and Northwest Shelf but relatively consistent stress orientations elsewhere. The rapid stress rotations in the Delaware Basin are observed in areas with relatively small differences between the horizontal stresses and with elevated pore pressure, making it easier for stress perturbations to cause significant changes in the stress field.

We show how the FSP software package can be used as a quantitative screening tool to estimate the fault slip potential in a region with large variations of the stress field, and accounting for uncertainties in stress measurements, rock properties, fault orientations, and fluid pressure. Although many historical earthquakes have occurred away from mapped faults in this area, we find that a number of earthquakes have occurred on or near faults for which there is high fault slip potential under the modeled conditions. TLE

Acknowledgments

The authors are grateful to Apache Corporation, Devon Energy, MicroSeismic Inc., and Pioneer Natural Resources, and to R. Cornell, for contributing new data. The authors also wish to thank F. R. Walsh III for providing scripts to assist with data handling and for helpful discussions. The authors appreciate thoughtful comments by B. Birkelo and prompt editorial assistance by J. Shemeta. This work was supported by the Stanford Center for Induced and Triggered Seismicity industrial affiliates program.

Corresponding author: lundsnee@stanford.edu

References

Alt, R. C. II, and M. D. Zoback, 2017, In situ stress and active faulting in Oklahoma: Bulletin of the Seismological Society of America, **107**, no. 1, 216–228, https://doi.org/10.1785/0120160156.

Cartwright, L. D. Jr., 1930, Transverse section of Permian Basin, west Texas and southeast New Mexico: AAPG Bulletin, **14**, 969–981.

Crone, A. J., and R. L. Wheeler, 2000, Data for Quaternary faults, liquefaction features, and possible tectonic features in the Central and Eastern United States, east of the Rocky Mountain front; U.S. Geological Survey Open-File Report.

Doser, D. I., M. R. Baker, M. Luo, P. Marroquin, L. Ballesteros, J. Kingwell, H. L. Diaz, and G. Kaip, 1992, The not so simple relationship between seismicity and oil production in the Permian Basin, west Texas: Pure and Applied Geophysics, **139**, no. 3-4, 481–506, https://doi.org/10.1007/BF00879948.

Doser, D. I., M. R. Baker, and D. B. Mason, 1991, Seismicity in the War-Wink gas field, Delaware Basin, west Texas, and its relationship to petroleum production: Bulletin of the Seismological Society of America, **81**, 971–986, https://doi.org/10.1016/0148-9062(92)93679-E.

Dutton, S. P., E. M. Kim, R. F. Broadhead, W. D. Raatz, C. L. Breton, S. C. Ruppel, and C. Kerans, 2005, Play analysis and leading-edge oil-reservoir development methods in the Permian Basin: Increased recovery-through advanced technologies: AAPG Bulletin, **89**, no. 5, 553–576, https://doi.org/10.1306/12070404093.

Ewing, T. E., R. T. Budnik, J. T. Ames, and D. M. Ridner, 1990, Tectonic map of Texas: Bureau of Economic Geology, University of Texas at Austin.

Fisher, N. I., T. Lewis, and B. J. J. Embleton, 1987, Statistical analysis of spherical data: Cambridge University Press.

Forand, D., V. Heesakkers, K. Schwartz, 2017, Constraints on natural fracture and in-situ stress trends of unconventional reservoirs in the Permian Basin, USA: Presented at Unconventional Resources Technology Conference.

Frohlich, C., H. R. DeShon, B. W. Stump, C. Hayward, M. J. Hornbach, and J. I. Walter, 2016, A historical review of induced earthquakes in Texas: Seismological Research Letters, **87**, no. 4, 1022–1038, https://doi.org/10.1785/0220160016.

Galley, J. E., 1958, Oil and geology in the Permian Basin of Texas and New Mexico: North America, *in* L. G. Weeks, ed., Habitat of Oil: AAPG, 395–446.

Gan, W., and C. Frohlich, 2013, Gas injection may have triggered earthquakes in the Cogdell oil field, Texas: Proceedings of the National Academy of Sciences of the United States of America, **110**, no. 47, 18786–18791, https://doi.org/10.1073/pnas.1311316110.

Green, G. N., and G. E. Jones, 1997, The digital geologic map of New Mexico in ARC/INFO format: U.S. Geological Survey Open-File Report.

Heidbach, O., M. Rajabi, K. Reiter, and M. Ziegler, 2016, The 2016 release of the world stress map, https://doi.org/10.5880/WSM.2016.002.

Herrmann, R. B., H. M. Benz, and C. J. Ammon, 2011, Monitoring the earthquake source process in North America: Bulletin of the Seismological Society of America, **101**, no. 6, 2609–2625, https://doi.org/10.1785/0120110095.

Herzog, M., 2014, Investigation of possible induced seismicity due to wastewater disposal in the Delaware Basin, Dagger Draw Field, New Mexico-Texas, USA: Honors thesis, University of Colorado.

Jing, H., H. Zhou, and A. Li, 2017, Microearthquakes in west Texas: Induced or not?: 87th Annual International Meeting, SEG, Expanded Abstracts, 5350–5355, https://doi.org/10.1190/segam2017-17749188.1.

Keller, G. R., A. Rogers, and C. D. Orr, 1987, Seismic activity in the Permian Basin area of west Texas and southeastern New Mexico, 1975–79: Seismological Research Letters, **58**, 63–70, https://doi.org/10.1785/gssrl.58.2.63.

Keller, G. R., A. M. Rogers, R. J. Lund, and C. D. Orr, 1981, A seismicity and seismotectonic study of the Kermit Seismic Zone, Texas: U.S. Geological Survey Open-File Report.

Kluth, C. F., and P. J. Coney, 1981, Plate tectonics of the Ancestral Rocky Mountains: Geology, **9**, no. 1, https://doi.org/10.1130/0091-7613(1981)9<10:PTOTAR>2.0.CO;2.

Lund, K., S. E. Box, C. Holm-Denoma, C. A. San Juan, R. J. Blakely, R. W. Saltus, E. D. Anderson, and E. H. Dewitt, 2015, Basement domain map of the conterminous United States and Alaska: U.S. Geological Survey Data Series 898, https://doi.org/10.3133/ds898.

Lund Snee, J.-E., and M. D. Zoback, 2016, State of stress in Texas: Implications for induced seismicity: Geophysical Research Letters, **43**, no. 19, 10,208–10,214, https://doi.org/10.1002/2016GL070974.

Matchus, E. J., and T. S. Jones, 1984, East-west cross section through Permian Basin of West Texas: West Texas Geological Society.

Moos, D., and M. D. Zoback, 1993, State of stress in the Long Valley caldera, California: Geology, **21**, no. 9, https://doi.org/10.1130/0091-7613(1993)021<0837:SOSITL>2.3.CO;2.

Orr, C. D., 1984, A seismotectonic study and stress analysis of the Kermit seismic zone: University of Texas at El Paso.

Pursley, J., S. L. Bilek, and C. J. Ruhl, 2013, Earthquake catalogs for New Mexico and bordering areas: 2005–2009: New Mexico Geology, **35**, 3–12.

Rittenhouse, S., J. Currie, R. Blumstein, 2016, Using mud weights, DST, and DFIT data to generate a regional pore pressure model for the Delaware Basin, New Mexico and Texas: Presented at Unconventional Resources Technology Conference.

Rogers, A. M., and A. Malkiel, 1979, A study of earthquakes in the Permian Basin of Texas-New Mexico: Bulletin of the Seismological Society of America, **69**, no. 3, 843–865.

Ruppel, S. C., R. H. Jones, C. L. Breton, and J. A. Kane, 2005, Preparation of maps depicting geothermal gradient and Precambrian structure in the Permian Basin: USGS Order no. 04CRSA0834 and Requisition no. 04CRPR01474.

Sanford, A. R., T. M. Mayeau, J. W. Schlue, R. C. Aster, and L. H. Jaksha, 2006, Earthquake catalogs for New Mexico and bordering areas II: 1999–2004: New Mexico Geology, **28**, 99–109.

Savvaidis, A., B. Young, P. Hennings, E. Rathje, G. Zalachoris, M. H. Young, J. I. Walter, H. R. DeShon, and C. Frohlich, 2017, Site assessment of a new state-wide seismic network in Texas (TexNet), USA, Presented at EGU General Assembly Conference.

Shumaker, R. C., 1992, Paleozoic structure of the Central Basin Uplift and adjacent Delaware Basin, west Texas: AAPG Bulletin, **76**, 1804–1824, https://doi.org/10.1306/BDFF8AD8-1718-11D7-8645000102C1865D.

Simpson, R. W., 1997, Quantifying Anderson's fault types: Journal of Geophysical Research, **102**, no. B8, 17909–17919, https://doi.org/10.1029/97JB01274.

Suter, M., 1991, State of stress and active deformation in Mexico and western Central America, *in* The Geology of North America Decade Map, v. 1, 401–421.

Thomas, W. A., 2006, Tectonic inheritance at a continental margin: GSA Today, **16**, no. 2, 4–11, https://doi.org/10.1130/1052-5173(2006)016[4:TIAACM]2.0.CO;2.

Tingay, M. R. P., B. Müller, J. Reinecker, and O. Heidbach, 2006, State and origin of the present-day stress field in sedimentary basins: New results from the world stress map project: Presented at 41st U.S. Symposium on Rock Mechanics.

Townend, J., and M. D. Zoback, 2000, How faulting keeps the crust strong: Geology, **28**, no. 5, 399–402, https://doi.org/10.1130/0091-7613(2000)28<399:HFKTCS>2.0.CO;2.

Walper, J. L., 1977, Paleozoic tectonics of the southern margin of North America: Gulf Coast Association of Geological Societies, **27**, 230–241.

Walsh, F. R. I., M. D. Zoback, D. Pais, M. Weingartern, and T. Tyrell, 2017, FSP 1.0: A program for probabilistic estimation of fault slip potential resulting from fluid injection, https://scits.stanford.edu/software, accessed 3 January 2018.

Walsh, F. R. I. III, and M. D. Zoback, 2016, Probabilistic assessment of potential fault slip related to injection-induced earthquakes: Application to north-central Oklahoma, USA: Geology, **44**, no. 12, 991–994, https://doi.org/10.1130/G38275.1.

Walsh, F. R. I. III, and M. D. Zoback, 2015, Oklahoma's recent earthquakes and saltwater disposal: Science Advances, **1**, no. 5, https://doi.org/10.1126/sciadv.1500195.

Xu, S., and M. D. Zoback, 2015, Analysis of stress variations with depth in the Permian Basin Spraberry/Dean/Wolfcamp Shale: American Rock Mechanics Association.

Yang, K.-M., and S. Dorobek, 1995, The Permian Basin of west Texas and New Mexico: Tectonic history of a "composite" foreland basin and its effects on stratigraphic development, *in* S. L. Dorobek and G. M. Ross, eds., Stratigraphic evolution of foreland basins: SEPM Publication, no. 52, 149–170, https://doi.org/10.2110/pec.95.52.0149.

Zhang, Y., M. Person, J. Rupp, K. Ellett, M. A. Celia, C. W. Gable, B. Bowen, J. Evans, K. Bandilla, P. Mozley, T. Dewers, and T. Elliot, 2013, Hydrogeologic controls on induced seismicity in crystalline basement rocks due to fluid injection into basal reservoirs: Ground Water, **51**, no. 4, 525–538, https://doi.org/10.1111/gwat.12071.

Zoback, M. L., 1992, First- and second-order patterns of stress in the lithosphere: The World Stress Map Project: Journal of Geophysical Research, **97**, no. B8, 11,703–11,728, https://doi.org/10.1029/92JB00132.

Zoback, M. D., 2010, Reservoir geomechanics: Cambridge University Press, https://doi.org/10.1017/CBO9780511586477.

Zoback, M. D., J. Townend, and B. Grollimund, 2002, Steady-state failure equilibrium and deformation of intraplate lithosphere: International Geology Review, **44**, no. 5, 383–401, https://doi.org/10.2747/0020-6814.44.5.383.

Zoback, M. L., and M. D. Zoback, 1989, Tectonic stress field of the continental United States: Geological Society of America, **172**, 523–540, https://doi.org/10.1130/MEM172-p523.

Zoback, M. L., and M. D. Zoback, 1980, State of stress in the conterminous United States: Journal of Geophysical Research, **85**, no. B11, 6113–6156, https://doi.org/10.1029/JB085iB11p06113.